CARBON 76 (2014) 459–463

Available at www.sciencedirect.com

ScienceDirect

journal homepage: www.elsevier.com/locate/carbon

Letter to the Editor

Forming-free resistive switching in a nanoporous nitrogen-doped carbon thin film with ready-made metal nanofilaments

Hao Chen [a,b], Fei Zhuge [b,*], Bing Fu [b], Jun Li [b], Jun Wang [c], Weigao Wang [c], Qin Wang [c], Le Li [c], Fagen Li [c], Haolei Zhang [b], Lingyan Liang [b], Hao Luo [b], Mei Wang [b], Junhua Gao [b], Hongtao Cao [b], Hong Zhang [a], Zhicheng Li [a,*]

[a] School of Materials Science and Engineering, Central South University, Changsha 410083, PR China
[b] Ningbo Institute of Materials Technology and Engineering, Chinese Academy of Sciences, Ningbo 315201, PR China
[c] Department of Physics, Ningbo University, Ningbo 315211, PR China

ARTICLE INFO

Article history:
Received 24 December 2013
Accepted 30 April 2014
Available online 14 May 2014

ABSTRACT

An amorphous carbon thin film, with through-pores of several tens of nanometers in size, has been synthesized by annealing magnetron sputtered nitrogen-doped carbon thin films at elevated temperature in an inert atmosphere. Based on this nanoporous carbon film, we first report forming-free resistive switching in a two terminal device containing ready-made metal nanofilaments. Such nanoporous carbon-based resistance memory device shows low operation voltages and good endurance and retention performance.

Resistive switching (RS) attributed to the formation/rupture of nanoscale metal (Cu, Ag, Au, or Ti) filaments has been reported in sputtered copper-doped carbon films [1–3], ion beam deposited hydrogenated carbon films [4], electron beam evaporated carbon films [5], and pulsed laser deposited nitrogen-doped diamond-like carbon films [6]. In these cases, an electrically [1–6] or thermally [7] induced metal filament formation process was necessary since no ready-made metal filaments existed in the pristine carbon films. Herein, we report forming-free RS phenomena in a nanoporous nitrogen-doped carbon thin film containing ready-made metal nanofilaments. The porous films have been synthesized by annealing magnetron sputtered N-doped carbon thin films at elevated temperature in an inert atmosphere.

Deposition of amorphous nitrogen-doped carbon thin films on commercial Pt/Ti/SiO_2/Si substrates was carried out by DC magnetron sputtering at room temperature (RT) in pure nitrogen. A high-purity pyrolytic graphite disc was used as the target. The composition of as-sputtered films was determined to be $CN_{0.25}$ by X-ray photoelectron spectroscopy (XPS). The atomic oxygen concentration was ~5 at.%. As-sputtered films were annealed at 600 °C in Ar ambient for 10 min. The annealed carbon films were still amorphous as determined by X-ray diffraction. The composition of annealed films was $CN_{0.15}$ with a very small amount of oxygen (~1 at.%). The thickness of as-sputtered ($CN_{0.25}$) and annealed ($CN_{0.15}$) carbon films was estimated to be ~60 and ~25 nm from the corresponding cross-sectional transmission electron

* *Corresponding authors.*
E-mail addresses: zhugefei@nimte.ac.cn (F. Zhuge), zhchli@csu.edu.cn (Z. Li).
http://dx.doi.org/10.1016/j.carbon.2014.04.091
0008-6223/

microscopy (TEM) images, as shown in Figs. S1a and b, respectively. The N 1s XPS spectra for $CN_{0.25}$ and $CN_{0.15}$ are shown in Figs. S2a and b, respectively. Both N 1s spectra can be deconvoluted into two distinct peaks at 398.6 and 400.2 eV. The peak at 398.6 eV can be assigned to N bonded to sp^3 coordinated C while the other peak at 400.2 eV can be assigned to N bonded to sp^2 coordinated C [8–10]. The N=Csp^2 bonds were found to be less stable than the N–Csp^3 bonds upon annealing [8,10]. In addition, a three-peak deconvolution of C 1s XPS spectra for $CN_{0.25}$ and $CN_{0.15}$ is shown in Figs. S2c and d. The peak at 284.4 eV corresponds to graphitic-like carbon while the peaks centred at 285.6 and 287.6 eV correspond to sp^2C=N and sp^3C–N bonds, respectively [8–10].

Atomic force microscopy (AFM) characterization was conducted to study the surface topography of as-sputtered and annealed carbon films. Fig. 1a and b shows the AFM images of $CN_{0.25}$ and $CN_{0.15}$, respectively. We see that the as-sputtered film has a smooth and dense surface without any pinhole whereas the annealed one contains numerous pores of several tens of nanometers in size. Further investigation on geometrical features of the nanopores in $CN_{0.15}$ films was provided by cross-sectional TEM (see Fig. 1c and d). The TEM specimen was prepared by focused ion beam (FIB) system using a finely focused beam of gallium ions. Protective layer of Pt was locally deposited on the $CN_{0.15}$ film to prevent beam-induced damage. More importantly, platinum, acting as the pore filler, could facilitate the TEM observation of nanopores. From the figure we can clearly observe an asymmetric through-pore filled with Pt with wider and narrower diameters of several tens of nanometers and several nanometers, respectively. We therefore conclude that numerous asymmetric nanosized through-pores were formed in annealed N-doped carbon thin films. For N-doped carbon films, it has been reported that a loss of N content accompanied by a film thickness reduction occurs as annealing at elevated temperatures due to the formation of volatile products such as N_2 and C_2N_2 [8–11]. Then, we can reasonably deduce that the formation of such volatile products also accounts for the growth of asymmetric through-nanopores.

In order to measure the electrical properties of $CN_{0.25}$ and $CN_{0.15}$ films, 50 nm thick Cu top electrodes of 100 μm in diameter were deposited at RT by electron-beam evaporation. To prevent Cu from oxidizing, ~20 nm thick Au protection layers were also deposited on the Cu electrodes. *I–V* characteristics of Cu/CN_x/Pt ($x = 0.25$ or 0.15) structures were measured at RT in air using a Keithley 4200 semiconductor parameter analyzer. The device structures are schematically illustrated in Fig. 2a and d. Fig. 2b and c plot the *I–V* curves of Cu/$CN_{0.25}$/Pt in linear and semilogarithmic scale, respectively. The *I–V* curves show typical bipolar RS characteristics. Based on our

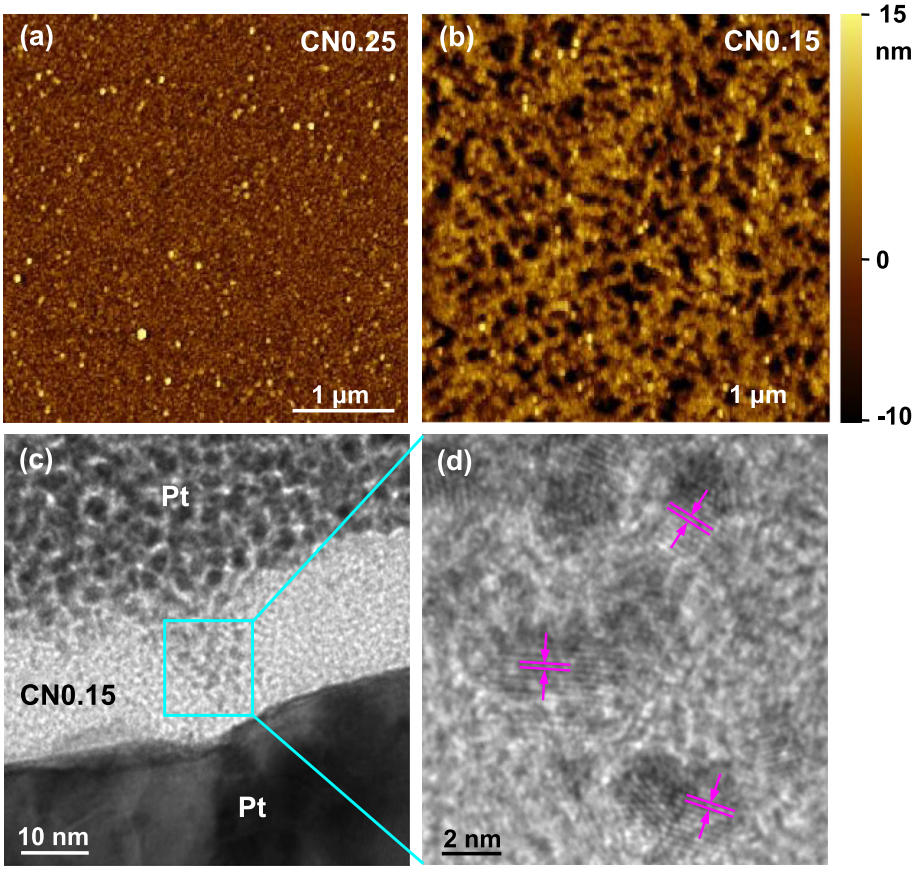

Fig. 1 – AFM images of (a) as-sputtered and (b) annealed nitrogen-doped carbon thin films. (c) Cross-sectional TEM image of the $CN_{0.15}$ thin film. The specimen was prepared by an FIB system. Protective layer of Pt was locally deposited on the film to prevent beam-induced damage. More importantly, Pt acts as the pore filler facilitating the observation of nanopores. A through-pore can be clearly observed. (d) High resolution TEM image for the area marked by the light blue rectangle. The lattice distance is 2.3 Å corresponding to the Pt (111) plane. (A colour version of this figure can be viewed online.)

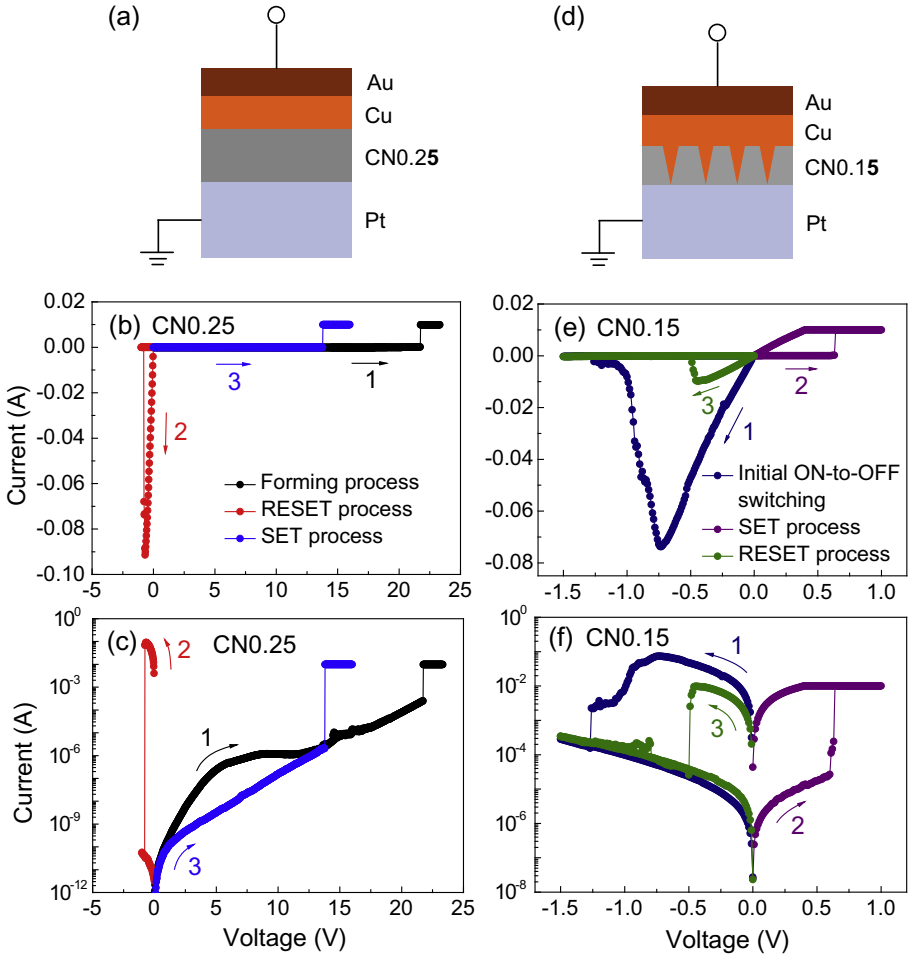

Fig. 2 – Schematic configurations for the two terminal resistive switching devices employing (a) as-sputtered and (d) annealed nitrogen-doped carbon thin films as the switching medium. *I–V* curves of Cu/$CN_{0.25}$/Pt in (b) linear and (c) semilogarithmic scale. *I–V* curves of Cu/$CN_{0.15}$/Pt in (e) linear and (f) semilogarithmic scale. In each figure, the arrows and numbers indicate the voltage sweeping sequence. (A colour version of this figure can be viewed online.)

previous studies on the RS in amorphous carbon and graphene oxide thin films [4,12], the RS mechanism of Cu/$CN_{0.25}$/Pt is suggested to be the formation/rupture of nanoscale Cu filaments. We see from Fig. 2 that an electroforming process with a voltage as large as +22 V is necessary for generating Cu nanofilaments in $CN_{0.25}$ thin films which connect the top and bottom electrodes switching Cu/$CN_{0.25}$/Pt from the pristine high resistance state (HRS or OFF-state) to a low resistance state (LRS or ON-state). The subsequent RESET (ON-to-OFF switching) and SET (OFF-to-ON switching) processes occur at −0.8 and +14 V, respectively. Cu/$CN_{0.15}$/Pt exhibits much different bipolar RS properties as shown in Fig. 2e or f. We see that the pristine Cu/$CN_{0.15}$/Pt is in an ON-state with a resistance as low as ~10 Ω. The initial ON-state can be switched to an OFF-state by applying a negative bias voltage with the absolute value larger than 0.7 V. The subsequent SET and RESET processes occur at +0.6 and −0.5 V, respectively. The Cu/$CN_{0.15}$/Pt devices have good endurance and retention properties at room temperature in air, as demonstrated in Fig. 3. From Fig. 3a and b showing the endurance performance, we can see, the LRS resistance and RESET voltage (V_{RESET}) are much more stable than the HRS resistance and SET voltage (V_{SET}) during more than 1000 *I–V* cycles. It is also worthy to note that the HRS resistance and V_{SET} exhibit narrower distributions after ~600 cycles.

The resistance of the pristine Cu/$CN_{0.15}$/Pt was measured as a function of temperature. Fig. 4a presents the resistance versus temperature plot. The resistance increases with temperature, showing a typical metallic behavior. The temperature dependence of metallic resistance can be written as $R(T) = R_0[1 + \alpha(T - T_0)]$, where R_0 is the resistance at temperature T_0, and α is the temperature coefficient of resistance. By choosing T_0 as 300 K, the α is calculated to be $3.0 \times 10^{-3}\,K^{-1}$, which is similar to the value $3.9 \times 10^{-3}\,K^{-1}$ for pure Cu. Given the presence of asymmetric through-nanopores in $CN_{0.15}$ and their capability to be filled with Pt, we can reasonably deduce that the nanopores were filled with Cu during the Cu evaporation process. Thus, there exist ready-made Cu nanofilaments connecting the top and bottom electrodes in the pristine Cu/$CN_{0.15}$/Pt, resulting in a metallic behavior, as schematically illustrated in Fig. 2d. The direct evidence on the existence of ready-made Cu nanofilaments was provided by cross-sectional TEM observations of Cu/$CN_{0.15}$/Pt, as shown in Fig. 4b–d. An asymmetric nanoscale filament with a similar

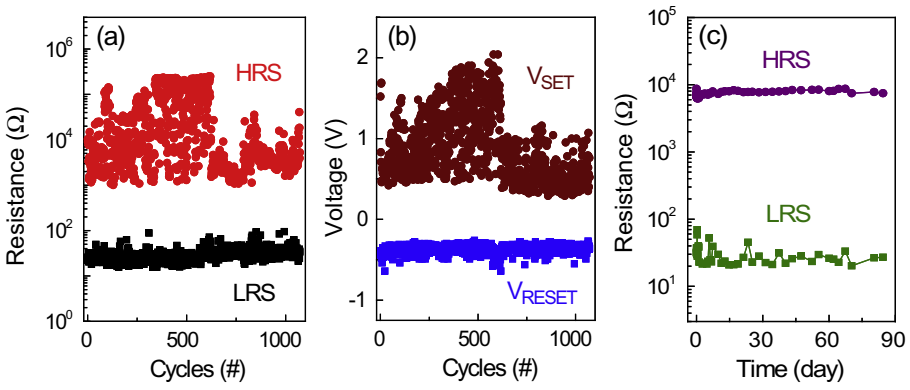

Fig. 3 – (a), (b) Endurance and (c) retention performance of Cu/$CN_{0.15}$/Pt. The measurements were conducted at RT in air. The resistance values were read at 0.1 V. (A colour version of this figure can be viewed online.)

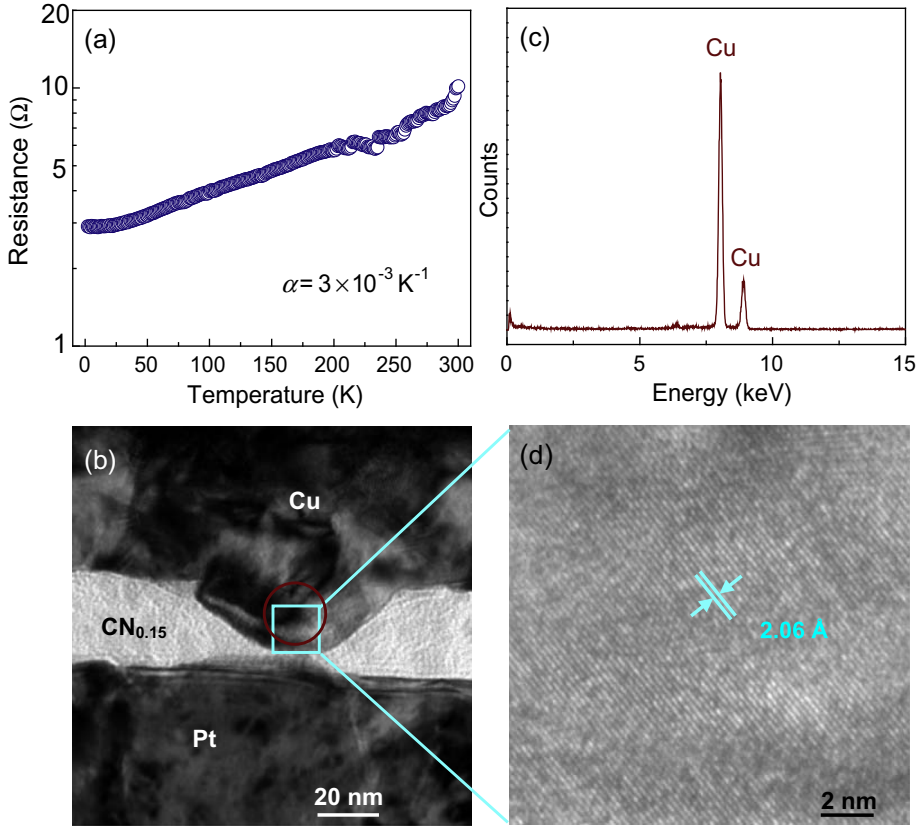

Fig. 4 – (a) Resistance versus temperature plot in semilogarithmic scale for the pristine Cu/$CN_{0.15}$/Pt devices. Also shown is the value of the temperature coefficient of resistance (α) calculated from the plot. (b) Cross-sectional TEM image of Cu/$CN_{0.15}$/Pt. Also shown are (c) EDX spectra for the area marked by the brown circle and (d) high resolution TEM image for the area marked by the light blue rectangle. The lattice distance 2.06 Å corresponds to the Cu (1 1 1) plane. (A colour version of this figure can be viewed online.)

shape to nanopores in $CN_{0.15}$ films can be seen very clearly in Fig. 4b. Both energy dispersive X-ray spectrometer (EDX) and high resolution TEM measurements indicate that the filament is composed of Cu. As applying a negative RESET voltage, the filaments near the $CN_{0.15}$/Pt interface with the highest electrical potential is electrochemically dissolved, switching the device to an OFF-state. The following SET process only needs to rejuvenate the previously ruptured filament segments, resulting in a low SET voltage, as illustrated in Fig. 2e or f [4,12]. Therefore, the RS occurs at the $CN_{0.15}$/Pt interface. As to the much broader distributions of the HRS resistance and SET voltage compared to the LRS resistance and RESET voltage during more than 1000 *I*–*V* cycles (see Fig. 3a and b), it is most likely due to a large cycle-to-cycle variation of the distance between the residual Cu filaments and Pt [13,14].

For comparison, we also deposited 50 nm thick Pt top electrodes of 100 μm in diameter onto $CN_{0.15}$ thin films by electron-beam evaporation. The pristine Pt/$CN_{0.15}$/Pt is in an ON-state and exhibits a resistance of ~11 Ω, indicating that there exist ready-made Pt nanofilaments in the pristine Pt/$CN_{0.15}$/Pt. However, the initial ON-state cannot be switched to an OFF-state as applying negative bias voltages and no RS phenomena can be observed (see Fig. S3). Given the high chemical activity of Cu while high chemical inertness of Pt, the much different electrical properties between Cu/$CN_{0.15}$/Pt and Pt/$CN_{0.15}$/Pt confirm that the RS occurring in Cu/$CN_{0.15}$/Pt originates from electrochemically induced rupture/re-formation of ready-made Cu nanofilaments. We can also exclude the possibility that the RS of Cu/$CN_{0.15}$/Pt is due to the electrochemical reactions induced by adsorbed water molecules in/on N-doped porous carbon thin films [12,15], or charge transfer reactions in porous carbon [16–21], since Cu/$CN_{0.15}$/Pt and Pt/$CN_{0.15}$/Pt show much different electrical behaviors.

Although we have not tried other porous films with through nanopores for resistance memory application, we believe that not any porous films with through nanopores filled with Cu metals show resistive switching behaviors. It should depend on the minimum diameter of through nanopores. If the minimum diameter is too large, i.e. the ready-made Cu nanofilaments are too thick, it is difficult to electrochemically dissolve the filaments as applying a negative RESET voltage. As a result, no resistive switching behaviors can be observed.

Acknowledgements

This work was supported by Chinese National Program on Key Basic Research Project (2012CB933003), National Natural Science Foundation of China (61006082, 51272261 and 51172287) and Science and Technology Innovative Research Team of Ningbo Municipality (2009B21005).

Appendix A. Supplementary data

Supplementary data associated with this article can be found, in the online version, at http://dx.doi.org/10.1016/j.carbon.2014.04.091.

REFERENCES

[1] Pyun M, Choi H, Park JB, Lee D, Hasan M, Dong R, et al. Electrical and reliability characteristics of copper-doped carbon (CuC) based resistive switching devices for nonvolatile memory applications. Appl Phys Lett 2008;93:212907.
[2] Kim DI, Yoon J, Park JB, Hwang H, Lim YM, Kwon SH, et al. Nonlinear current–voltage behavior of the isolated resistive switching filamentary channels in CuC nanolayer. Appl Phys Lett 2011;98:152107.
[3] Choi H, Pyun M, Kim TW, Hasan M, Dong R, Lee J, et al. Nanoscale resistive switching of a copper–carbon-mixed layer for nonvolatile memory applications. IEEE Electron Dev Lett 2009;30:302–4.
[4] Zhuge F, Dai W, He CL, Wang AY, Liu YW, Li M, et al. Nonvolatile resistive switching memory based on amorphous carbon. Appl Phys Lett 2010;96:163505.
[5] Chai Y, Wu Y, Takei K, Chen HY, Yu SM, Chan PCH, et al. Nanoscale bipolar and complementary resistive switching memory based on amorphous carbon. IEEE Trans Electron Devices 2011;58:3933–9.
[6] Peng PG, Xie D, Yang Y, Zang YY, Gao XL, Zhou CJ, et al. Resistive switching behavior in diamond-like carbon films grown by pulsed laser deposition for resistance switching random access memory application. J Appl Phys 2012;111:084501.
[7] Lee W, Park J, Kim S, Woo J, Shin J, Lee D, et al. Improved switching uniformity in resistive random access memory containing metal-doped electrolyte due to thermally agglomerated metallic filaments. Appl Phys Lett 2012;100:142106.
[8] Fernández-Ramos C, Sayagués MJ, Rojas TC, Alcalá MD, Real C, Fernández A. Study of the thermal stability of carbon nitride thin films prepared by reactive magnetron sputtering. Diamond Relat Mater 2000;9:212–8.
[9] Hellgren N, Lin N, Broitman E, Serin V, Grillo SE, Twesten R, et al. Thermal stability of carbon nitride thin films. J Mater Res 2001;16:3188–201.
[10] Li JJ, Zheng WT, Jin ZS, Gai TX, Gu GR, Bian HJ, et al. Thermal stability of magnetron sputtering amorphous carbon nitride films. Vacuum 2004;72:233–9.
[11] Falk F, Meinschien J, Schuster K, Stafast H. Properties and preparation conditions of carbon nitride thin films deposited by laser CVD. Carbon 1998;36:765–9.
[12] Zhuge F, Hu BL, He CL, Zhou XF, Liu ZP, Li RW. Mechanism of nonvolatile resistive switching in graphene oxide thin films. Carbon 2011;49:3796–802.
[13] Liu Q, Sun J, Lv HB, Long SB, Yin KB, Wan N, et al. Real-time observation on dynamic growth/dissolution of conductive filaments in oxide-electrolyte-based ReRAM. Adv Mater 2012;24:1844–9.
[14] Peng SS, Zhuge F, Chen XX, Zhu XJ, Hu BL, Pan L, et al. Mechanism for resistive switching in an oxide-based electrochemical metallization memory. Appl Phys Lett 2012;100:072101.
[15] Mativetsky JM, Treossi E, Orgiu E, Melucci M, Veronese GP, Samori P, et al. Local current mapping and patterning of reduced graphene oxide. J Am Chem Soc 2010;132:14130–6.
[16] Lin WP, Liu SJ, Gong T, Zhao Q, Huang W. Polymer-based resistive memory materials and devices. Adv Mater 2014;26:570–606.
[17] Chen Y, Zhang B, Liu G, Zhuang XD, Kang ET. Graphene and its derivatives: switching ON and OFF. Chem Soc Rev 2012;41:4688–707.
[18] Son DI, Park DH, Kim JB, Choi JW, Kim TW, Angadi B, et al. Bistable organic memory device with gold nanoparticles embedded in a conducting poly(N-vinylcarbazole) colloids hybrid. J Phys Chem C 2011;115:2341–8.
[19] Liu SJ, Wang P, Zhao Q, Yang HY, Wong J, Sun HB, et al. Single polymer-based ternary electronic memory material and device. Adv Mater 2012;24:2901–5.
[20] Zhuang XD, Chen Y, Liu G, Zhang B, Neoh KG, Kang ET, et al. Preparation and memory performance of a nanoaggregated dispersed red 1-functionalized poly(N-vinylcarbazole) film via solution-phase self-assembly. Adv Funct Mater 2010;20:2916–22.
[21] Zhuang XD, Chen Y, Liu G, Li PP, Zhu CX, Kang ET, et al. Conjugated-polymer-functionalized graphene oxide: synthesis and nonvolatile rewritable memory effect. Adv Mater 2010;22:1731–5.